

Scaling properties of multilayer random networks

J. A. Méndez-Bermúdez,¹ Guilherme Ferraz de Arruda,^{2,3} Francisco A. Rodrigues,² and Yamir Moreno^{3,4,5}

¹*Instituto de Física, Benemérita Universidad Autónoma de Puebla, Apartado Postal J-48, Puebla 72570, Mexico*

²*Departamento de Matemática Aplicada e Estatística, Instituto de Ciências Matemáticas e de Computação, Universidade de São Paulo-Campus de São Carlos, Caixa Postal 668, 13560-970 São Carlos, SP, Brazil*

³*Institute for Biocomputation and Physics of Complex Systems (BIFI), University of Zaragoza, Zaragoza 50009, Spain*

⁴*Department of Theoretical Physics, University of Zaragoza, Zaragoza 50009, Spain*

⁵*Complex Networks and Systems Lagrange Lab, Institute for Scientific Interchange, Turin, Italy*

(Received 21 November 2016; revised manuscript received 22 March 2017; published 7 July 2017)

Multilayer networks are widespread in natural and manmade systems. Key properties of these networks are their spectral and eigenfunction characteristics, as they determine the critical properties of many dynamics occurring on top of them. Here, we numerically demonstrate that the normalized localization length β of the eigenfunctions of multilayer random networks follows a simple scaling law given by $\beta = x^*/(1 + x^*)$, with $x^* = \gamma(b_{\text{eff}}^2/L)^\delta$, $\delta \sim 1$, and b_{eff} being the effective bandwidth of the adjacency matrix of the network, whose size is L . The scaling law for β , that we validate on real-world networks, might help to better understand criticality in multilayer networks and to predict the eigenfunction localization properties of them.

DOI: [10.1103/PhysRevE.96.012307](https://doi.org/10.1103/PhysRevE.96.012307)

I. INTRODUCTION

Real systems are naturally structured in levels or interconnected substructures, which in turn consists of nodes organized in networks [1]. For instance, individuals are connected through different social circles, each of which can be thought of as a network. People and goods are transported through different mobility modes, such as airlines, roads, and ships. These systems are nowadays referred to as multilayer networks [1,2]. The study of these systems is important as many critical properties of several phenomena are determined by the topology of them, and specifically by the spectral and eigenfunction properties of the adjacency and the Laplacian matrices of the networks. One particularly suitable approach to address the relation between the structure and the dynamics of a networked system is given by random matrix theory (RMT). RMT has numerous applications in many different fields, from condensed matter physics to financial markets [3]. In the case of complex networks, the use of RMT techniques might reveal universal properties [4], which are always of interest, as they allow to reduce the set of parameters describing the system and provide relations that allow to deduce its behavior from those few global parameters.

In this paper, we study whether there are universal scaling properties in multilayer systems. We perform a scaling analysis of the eigenfunction localization properties of multilayer networks using RMT models and techniques. We explore multilayer networks whose networks of layers [2] are of two types: (i) a line and (ii) a complete graph (node-aligned multiplex networks). In the first case, we study weighted layers coupled by weighted matrices, whereas in the latter case, weighted and binary layers coupled by identity matrices are considered. We demonstrate that the normalized localization length of the eigenfunctions of multilayer random networks exhibits a well defined scaling function and also test the scaling law on real-world networks. Our results can be used to predict or design the localization features of the eigenfunctions of multilayer random networks and to better understand critical properties that depend on eigenfunction properties.

II. MODEL DEFINITION AND PROBLEM STATEMENT

A multilayer network is formed by M undirected random layers with corresponding adjacency matrices $A^{(m)}$ having N_m nodes each. The respective adjacency matrix of the whole network is expressed by $\mathbf{A} = \bigoplus_{m=1}^M A^{(m)} + p\mathbf{C}$, where \bigoplus represents the direct sum, p is a parameter that defines the strength of the interlayer edges, and \mathbf{C} is the interlayer coupling matrix, whose elements represent the relations between nodes in different layers, thus implicitly containing the information of a network of layers [7]. Examples of multilayers are shown in Fig. 1. Observe that the spectra of the adjacency matrix \mathbf{A} is a function of the parameter p . As a consequence, eigenvalue crossings, structural transitions [8], near crossings [9], or localization problems [9,10] are inherent to the network spectra, depending on p for multilayer networks. Regarding dynamical processes, p plays a fundamental role. For instance, in diffusion processes, it can drive the multilayer system to a superdiffusion regime [11]. Likewise, in contagion dynamics, in which p is associated to the ratio of intralayer and interlayer spreading rates, there can be both localized and delocalized states [9] depending on the value of p . Here, we restrict ourselves to $p = 1$: for $p \ll 1$ the layers can be considered as uncoupled, while for $p \gg 1$ the topology of the network of layers dominates the spectral properties [7,8]. In this way, $p = 1$ represents a suitable intermediary case (multilayer phase).

We define two ensembles of multilayer random networks as adjacency matrices. As the first model we consider a network of layers on a line [see Fig. 1(a)], whose adjacency matrix \mathbf{A} has the form

$$\mathbf{A} = \begin{pmatrix} A^{(1)} & C^{(1,2)} & \dots & 0 \\ C^{(2,1)} & A^{(2)} & & 0 \\ \vdots & & \ddots & C^{(M-1,M)} \\ 0 & 0 & C^{(M,M-1)} & A^{(M)} \end{pmatrix}, \quad (1)$$

where $(C^{(m,m')})_{i,j} = (C^{(m,m')})_{j,i}^T$ are real rectangular matrices of size $N_m \times N_{m'}$ and 0 represents null matrices.

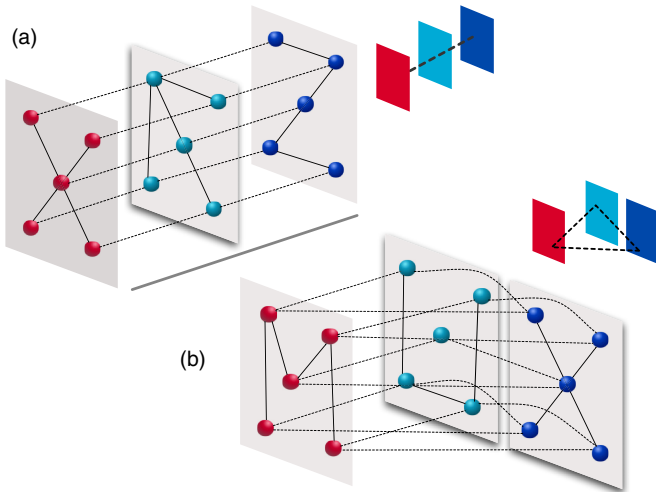


FIG. 1. Illustration of the two types of multilayer networks studied here. The network of layers are (a) a line and (b) a complete network. Here, each network is composed by $M = 3$ layers having $N = 5$ nodes.

Furthermore, we consider a special class of matrices $A^{(m)}$ and $C^{(m,m')}$ which are characterized by the sparsities α_A and α_C , respectively. In other words, since with a probability α_* their elements can be removed, these matrices represent Erdős-Rényi-type random networks. Notice that when the N_m are all the same $N_m = \text{const} \equiv N$, which is the case we explore here. Also, the adjacency matrix \mathbf{A} has the structure of a block-banded matrix of size $L = M \times N$. In addition, we consider this model as a model of weighted networks, i.e., the nonvanishing elements $A_{i,j}$ are independent Gaussian variables with zero mean and variance $1 + \delta_{i,j}$. We justify the addition of self-loops and random weights to edges by recognizing that in real-world networks the nodes and the interactions between them are in general nonequivalent. Moreover, with this prescription we retrieve well known random matrices [12] in the appropriate limits: a diagonal random matrix is obtained for $\alpha_A = \alpha_C = 0$ (Poisson case), whereas the Gaussian orthogonal ensemble (GOE) is recovered when $\alpha_A = \alpha_C = 1$ and $M = 2$. For simplicity, and without loss of generality, in this work we consider the case where $\alpha \equiv \alpha_A = \alpha_C$. As an example, this network model can be applied to transportation networks, where the interlayer edges represent connections between two different means of transport. An obvious constraint is that no layer can be connected to more than two layers. In addition to the above configuration, we are also interested on the node-aligned multiplex case, whose network of layers is a complete graph [see Fig. 1(b)].

There is a well known RMT model known as the banded random matrix (BRM) model which was originally introduced to emulate quasi-one-dimensional disordered wires of length L and width b (with $b \ll L$). The BRM ensemble is defined as the set of $L \times L$ real symmetric matrices whose entries are independent Gaussian random variables with zero mean and variance $1 + \delta_{i,j}$ if $|i - j| < b$ and zero otherwise. Therefore, b is the number of nonzero elements in the first matrix row which equals 1 for diagonal, 2 for tridiagonal, and L

for matrices of the GOE. There are several numerical and theoretical studies available for this model (see, for example, Refs. [13–27]). In particular, outstandingly, it has been found [13–20] that the eigenfunction properties of the BRM model, characterized by the *scaled localization length* β , are *universal* for the fixed ratio $x = b^2/L$. More specifically, it was numerically and theoretically shown that the scaling function

$$\beta = \frac{\gamma^x}{1 + \gamma x}, \quad (2)$$

with $\gamma \sim 1$, holds for the BRM model. Admittedly, the ensemble of adjacency matrices of the multilayer network with layers on a line [see Eq. (1)] can be considered as a *nonhomogeneous diluted version* of the BRM model. Therefore, motivated by the similarity between these two matrix models, we propose the study of eigenfunction properties of the adjacency matrices of multilayer and multiplex random networks as a function of the parameter

$$x = \frac{b_{\text{eff}}^2}{L}, \quad (3)$$

where $b_{\text{eff}} \equiv b_{\text{eff}}(N, \alpha)$ is the adjacency matrix effective bandwidth and $L = M \times N$.

A commonly accepted tool to characterize quantitatively the complexity of the eigenfunctions of random matrices (and of Hamiltonians corresponding to disordered and quantized chaotic systems) is the information or Shannon entropy S . This measure provides the number of principal components of an eigenfunction in a given basis. In fact, S has been already used to characterize the eigenfunctions of the adjacency matrices of random network models; see some examples in Refs. [6,28–32]. The Shannon entropy for the eigenfunction Ψ^l is given as $S = -\sum_{n=1}^L (\Psi_n^l)^2 \ln(\Psi_n^l)^2$ and allows computing the scaled localization length as [33]

$$\beta = \exp(\langle S \rangle - S_{\text{GOE}}), \quad (4)$$

where $S_{\text{GOE}} \approx \ln(L/2.07)$, used as a reference, is the entropy of a random eigenfunction with Gaussian distributed amplitudes (i.e., an eigenfunction of the GOE). With this definition [34], β can take values in the range (0, 1]. Here, as well as in BRM model studies, we look for the scaling properties of the eigenfunctions of our random network models through β [35].

III. SCALING ANALYSIS OF MULTILAYER NETWORKS

We now analyze in detail the multilayer network model with adjacency matrix given by Eq. (1). In Fig. 2(a), we present β as a function of x [see Eq. (3)] for ensembles of networks characterized by the sparsity α . We have defined b_{eff} as the average number of nonvanishing elements per adjacency-matrix row

$$b_{\text{eff}} = 2N\alpha. \quad (5)$$

We observe that the curves of β versus x in Fig. 2(a) have a functional form similar to that for the BRM model. To show this, we are including Eq. (2) (black dashed line) with $\gamma = 1.4$ (the value of γ reported in Ref. [13] for the BRM model) which is very close to our data for $\alpha = 0.8$. In addition, in Fig. 2(b) the logarithm of $\beta/(1 - \beta)$ as a function of $\ln(x)$ is presented. The quantity $\beta/(1 - \beta)$ was useful in the study

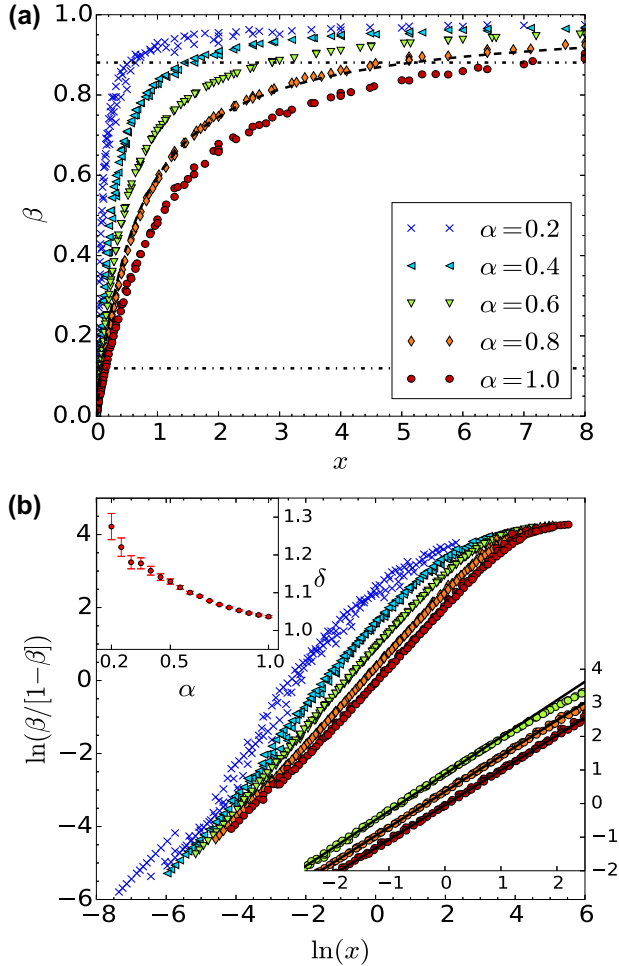


FIG. 2. (a) Scaled localization length β as a function of $x = b_{\text{eff}}^2/L$ for ensembles of multilayer networks characterized by the sparsity α . The dashed line close to the data for $\alpha = 0.8$ is Eq. (2) with $\gamma = 1.4$. Horizontal dotted-dashed lines at $\beta \approx 0.12$ and 0.88 are shown as a reference (see the text). (b) Logarithm of $\beta/(1 - \beta)$ as a function of $\ln(x)$. Upper inset: power δ , from the fittings of the data with Eq. (6), as a function of α . Lower inset: enlargement in the range $\ln[\beta/(1 - \beta)] = [-2, 4]$ including data for $\alpha = 0.6, 0.8$, and 1 . Lines are fittings of the data using Eq. (6).

of the scaling properties of the BRM model [13,16] because $\beta/(1 - \beta) = \gamma x$, which is equivalent to scaling (2), implies that a plot of $\ln[\beta/(1 - \beta)]$ versus $\ln(x)$ is a straight line with unit slope. Even though, this statement is valid for the BRM model in a wide range of parameters {i.e., for $\ln[\beta/(1 - \beta)] < 2$ } it does not apply to our multilayer random network model [see Fig. 2(b)]. In fact, from this figure we observe that plots of $\ln[\beta/(1 - \beta)]$ versus $\ln(x)$ are straight lines (in a wide range of x) with a slope that depends on the sparsity α . Therefore, we propose the scaling law

$$\frac{\beta}{1 - \beta} = \gamma x^\delta, \quad (6)$$

where both γ and δ depend on α . Indeed, Eq. (6) describes well our data, mainly in the range $\ln[\beta/(1 - \beta)] = [-2, 2]$, as can be seen in the inset of Fig. 2(b) where we show the numerical data for $\alpha = 0.6, 0.8$, and 1 and include fittings through Eq. (6).

We stress that the range $\ln[\beta/(1 - \beta)] = [-2, 2]$ corresponds to a reasonable large range of β values, $\beta \approx [0.12, 0.88]$, whose bounds are indicated with horizontal dotted-dashed lines in Fig. 2(a). Finally, we notice that the power δ , obtained from the fittings of the data using Eq. (6), is very close to unity for all the sparsity values we consider here [see the upper inset of Fig. 2(b)].

Therefore, from the analysis of the data in Fig. 2, we are able to write a *universal scaling function* for the scaled localization length β of the eigenfunctions of our multilayer random network model as

$$\frac{\beta}{1 - \beta} = x^*, \quad (7)$$

where the scaling parameter $x^* = \gamma x^\delta$, as a function of the multilayer network parameters, is given by

$$x^* \equiv \gamma \left(\frac{4N\alpha^2}{M} \right)^\delta. \quad (8)$$

To validate Eq. (7) in Fig. 3(b) we present again the data for $\ln[\beta/(1 - \beta)]$ shown in Fig. 2(b) but now as a function of $\ln(x^*)$. We do observe that curves for different values of α fall on top of Eq. (7) for a wide range of the variable x^* . Moreover, the collapse of the numerical data is excellent in the range $\ln[\beta/(1 - \beta)] = [-2, 2]$ for $\alpha \geq 0.5$, as shown in the inset of Fig. 3(b). Additionally, we rewrite Eq. (7) into the equivalent, but explicit, scaling function for β :

$$\beta = \frac{x^*}{1 + x^*}. \quad (9)$$

In Fig. 3(a), we confirm the validity of Eq. (9). We emphasize that the universal scaling given in Eq. (9) extends outside the range $\beta \approx [0.12, 0.88]$, for which Eq. (6) was shown to be valid [see the main panel of Fig. 3(a)]. Clearly, the collapse of the numerical data following Eq. (9) is remarkably good for $\alpha \geq 0.5$, as shown in the inset of Fig. 3(a).

Furthermore, we verify below that scaling (9) is also applicable to node-aligned multiplex networks, which are relevant for certain applications, once b_{eff} is properly defined.

IV. SCALING ANALYSIS OF MULTIPLEX NETWORKS

In the node-aligned multiplex case, whose network of layers is a complete graph, the coupling matrices are restricted to identity matrices and all layers have the same number of nodes [see Fig. 1(b)]. The adjacency matrix of a node-aligned multiplex is given as

$$\mathbf{A} = \begin{pmatrix} A^{(1)} & I & I & \cdots & I \\ I & A^{(2)} & I & & I \\ I & I & A^{(3)} & & I \\ \vdots & & & \ddots & I \\ I & I & I & I & A^{(M)} \end{pmatrix}. \quad (10)$$

Similarly to the multilayer model of Eq. (1), this configuration is characterized by the sparsity α which we choose to be constant for all the M matrices $A^{(m)}$ of size $N \times N$ composing the adjacency matrix \mathbf{A} of size $L = M \times N$. Additionally, the configuration (10) is considered in two different setups: weighted and unweighted multiplex without self-loops. In the

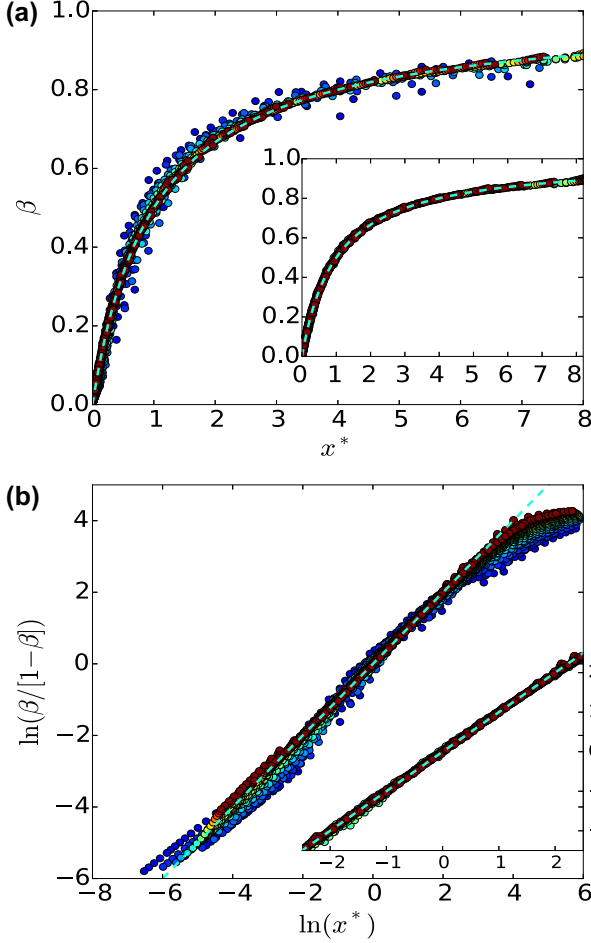


FIG. 3. (a) β as a function of x^* [as defined in Eq. (8)] for ensembles of multilayer networks with $\alpha \in [0.2, 1]$ in steps of 0.05. Inset: data for $\alpha \in [0.5, 1]$ in steps of 0.05. Dashed lines are Eq. (9). (b) Logarithm of $\beta/(1 - \beta)$ as a function of $\ln(x^*)$ for $\alpha \in [0.2, 1]$ in steps of 0.05. Inset: enlargement in the range $\ln[\beta/(1 - \beta)] = [-2, 2]$ including curves for $\alpha \in [0.5, 1]$ in steps of 0.05. Dashed lines are Eq. (7).

weighted case, the nonvanishing elements of the matrices $A^{(m)}$ are chosen as independent Gaussian variables with zero mean and variance $1 + \delta_{i,j}$. A realistic example of this configuration are online social systems, where each layer represents a different online network (e.g., Facebook, Twitter, and Google+, etc). In the unweighted case, the nonvanishing elements of $A^{(m)}$ are equal to unity. In (10), I are identity matrices of size $N \times N$.

A. Weighted multiplex

Now, we consider weighted multiplex networks (i.e., where the nonvanishing elements of the adjacency matrices $A^{(m)}$ in (10) are chosen as independent Gaussian variables with zero mean and variance $1 + \delta_{i,j}$). We follow the same methodology as in the multilayer case. Thus, in Fig. 4(a) we first present curves of β versus x ; however, we redefine b_{eff} as

$$b_{\text{eff}} = N\alpha, \quad (11)$$

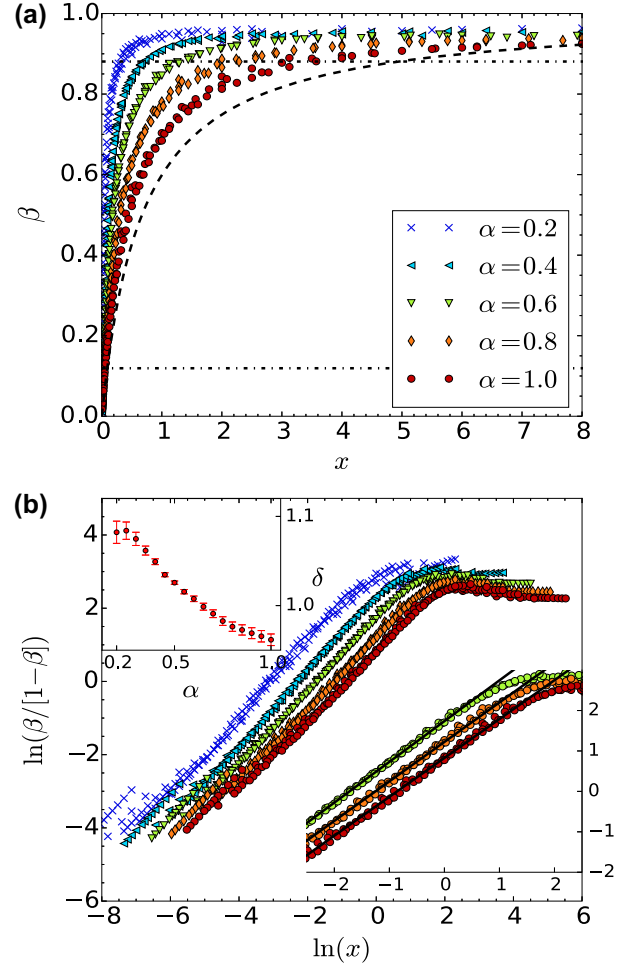


FIG. 4. (a) Scaled localization length β as a function of $x = b_{\text{eff}}^2/L$ for ensembles of weighted multiplex networks characterized by the sparsity α . The black dashed line corresponds to Eq. (2) with $\gamma = 1.4$. Horizontal black dotted-dashed lines at $\beta \approx 0.12$ and 0.88 are shown as a reference (see the text). (b) Logarithm of $\beta/(1 - \beta)$ as a function of $\ln(x)$. Upper inset: power δ , from the fittings of the data with Eq. (6), as a function of α . Lower inset: enlargement in the range $\ln[\beta/(1 - \beta)] = [-2, 2]$ including data for $\alpha = 0.6, 0.8$, and 1. Lines are fittings of the data with Eq. (6).

which is the average number of nonvanishing elements per row inside the adjacency-matrix band in the multiplex setup. From Fig. 4(a) we observe that the curves of β versus x have functional forms similar to those for the multilayer model [compare with Fig. 2(a)], however, with larger values of β for given values of x . As a reference we also include Eq. (2) (black dashed line) with $\gamma = 1.4$, corresponding to the BRM model, which is even below the data for $\alpha = 1$. Moreover, in Fig. 4(b) we show the logarithm of $\beta/(1 - \beta)$ as a function of $\ln(x)$. As in the multilayer case, here we observe that plots of $\ln[\beta/(1 - \beta)]$ versus $\ln(x)$ are straight lines mainly in the range $\ln[\beta/(1 - \beta)] = [-2, 2]$ with a slope that depends on the sparsity α . We indicate the bounds of this range with horizontal dotted-dashed lines in Fig. 4(a). Therefore, the scaling law of Eq. (6) is also valid here. Indeed, in the upper inset of Fig. 4(b) we report the power δ obtained from fittings of the data with Eq. (6).

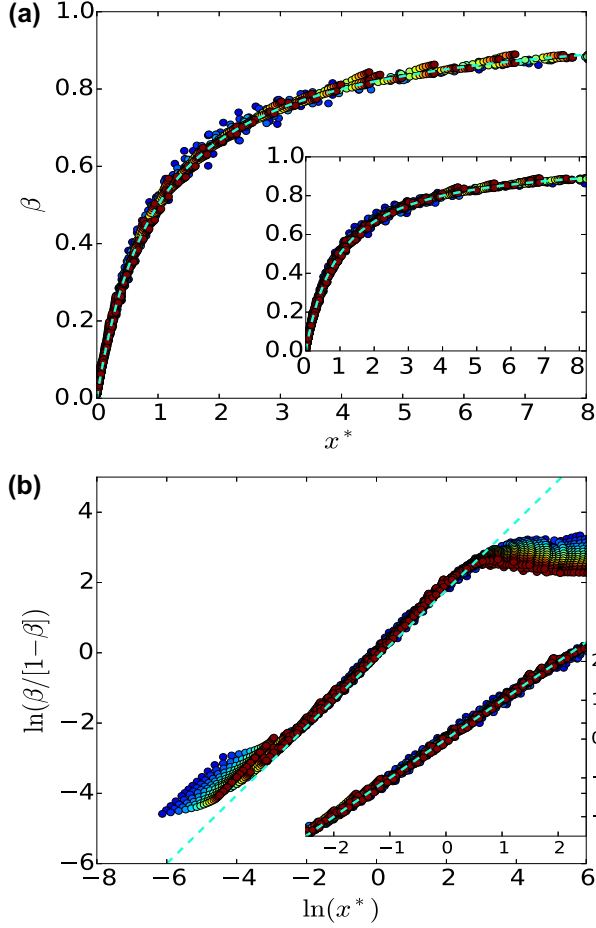


FIG. 5. (a) β as a function of x^* [as defined in Eq. (8)] for ensembles of weighted multiplex networks with $\alpha \in [0.2, 1]$ in steps of 0.05. Inset: Data for $\alpha \in [0.5, 1]$ in steps of 0.05. Dashed lines in main panel and inset are Eq. (9). (b) Logarithm of $\beta/(1-\beta)$ as a function of $\ln(x^*)$ for $\alpha \in [0.2, 1]$ in steps of 0.05. Inset: Enlargement in the range $\ln[\beta/(1-\beta)] = [-2, 2]$ including curves for $\alpha \in [0.5, 1]$ in steps of 0.05. Dashed lines in main panel and inset are Eq. (7).

In order to validate the scaling hypothesis of Eq. (7) for the node-aligned multiplex setup, in Fig. 5(b) we present the data for $\ln[\beta/(1-\beta)]$ shown in Fig. 4(b), but now as a function of $\ln(x^*)$. We observe that curves for different values of α fall on top of Eq. (7) for a wide range of the variable x^* . Moreover, the collapse of the numerical data on top of Eq. (7) is excellent in the range $\ln[\beta/(1-\beta)] = [-2, 2]$ for $\alpha \geq 0.5$, as shown in the inset of Fig. 5(b). Finally, in Fig. 5(a) we confirm the validity of Eq. (9) which is as good here as for the multilayer case. We emphasize that the collapse of the numerical data on top of Eq. (9) is remarkably good for $\alpha \geq 0.5$, as shown in the inset of Fig. 5(a).

B. Unweighted multiplex

The last analyzed scenario is the binary multiplex case. We recall that, in contrast to the two previous random network models, this model does not include weighted self-loops. Therefore, the Poisson limit is not recovered when $\alpha \rightarrow 0$ and β is not well defined there. Thus, we will compute β for values of x as smaller as the adjacency-matrix diagonalization

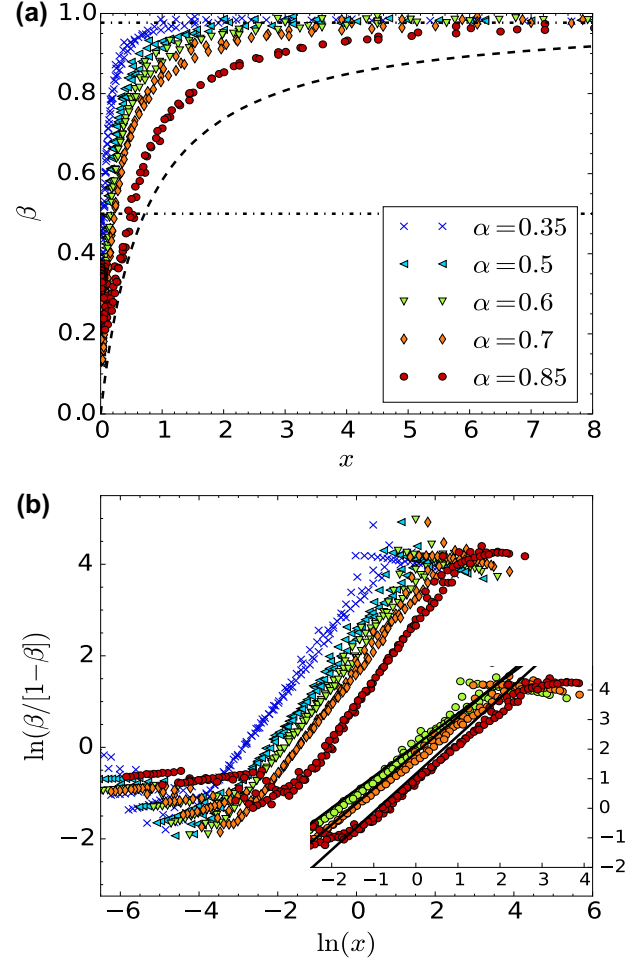


FIG. 6. (a) Scaled localization length β as a function of $x = b_{\text{eff}}^2/L$ for ensembles of unweighted multiplex networks characterized by the sparsity α . The black dashed line corresponds to Eq. (2) with $\gamma = 1.4$. Horizontal black dotted-dashed lines at $\beta \approx 0.5$ and 0.98 are shown as a reference (see the text). (b) Logarithm of $\beta/(1-\beta)$ as a function of $\ln(x)$. Lower inset: enlargement in the range $\ln[\beta/(1-\beta)] = [-2, 4]$ including data for $\alpha = 0.6, 0.7, 0.85$. Lines are fittings of the data with Eq. (6).

produces meaningful results. Also, as for the weighted multiplex, we use here the effective bandwidth given in Eq. (11).

The conducted experiments are similar to the previous ones. Then, in Figs. 6(a) and 6(b) we present curves of β versus x and $\ln[\beta/(1-\beta)]$ versus $\ln(x)$, respectively. Here, due to the absence of self-loops, we observe important differences with respect to the previous cases: In particular, the curves β versus x present minima at given small values of x . This feature can be seen clearer in Fig. 6(b) since it is magnified there. Also, from Fig. 6(b) we can notice that the range where $\ln[\beta/(1-\beta)]$ is a linear function of $\ln(x)$ has been shifted upwards for all the values of α considered. Therefore, we perform fittings to the curves $\ln[\beta/(1-\beta)]$ versus $\ln(x)$ with Eq. (6) in the interval $\ln[\beta/(1-\beta)] = [0, 3.75]$; the bounds of this interval are marked as dotted-dashed lines in Fig. 6(a). The corresponding values of δ are reported in Fig. 9(a). Now, under the above conditions, we validate our scaling hypothesis by plotting β versus x^* and $\ln[\beta/(1-\beta)]$ versus $\ln(x^*)$

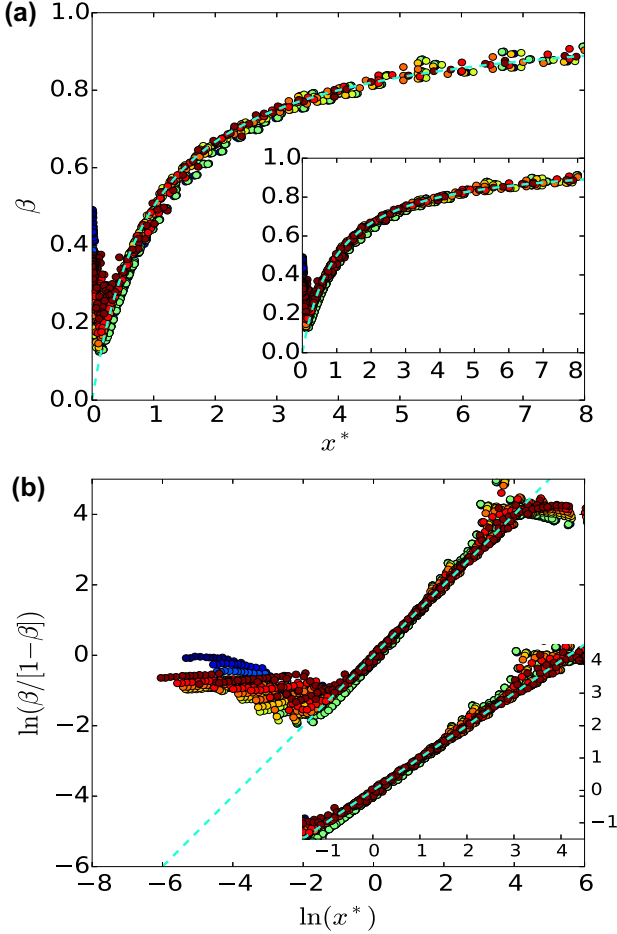


FIG. 7. (a) β as a function of x^* [as defined in Eq. (8)] for ensembles of unweighted multiplex networks with $\alpha \in [0.2, 1]$ in steps of 0.05. Inset: data for $\alpha \in [0.5, 1]$ in steps of 0.05. Dashed lines in main panel and inset are Eq. (9). (b) Logarithm of $\beta/(1-\beta)$ as a function of $\ln(x^*)$ for $\alpha \in [0.2, 1]$ in steps of 0.05. Inset: enlargement in the range $\ln[\beta/(1-\beta)] = [-1, 4]$ including curves for $\alpha \in [0.5, 1]$ in steps of 0.05. Dashed lines in main panel and inset are Eq. (7).

[see Figs. 7(a) and 7(b), respectively]. Remarkably, we observe a clear scaling behavior also in the unweighted multiplex case (despite the minima in the curves β versus x^* for small x^*).

V. APPLICATION TO REAL-WORLD NETWORKS

Finally, we test the scaling law for β for a number of real-world multiplex networks (see Table I and Appendix).

TABLE I. Parameter values of the networks reported in Fig. 8.

Network name	N	M	$\bar{\alpha}$	x^*
Kapferer tailor shop [36] (○)	39	4	0.1862	29.417
Oryctolagus genetic [37,38] (□)	144	3	0.0044	0.1056
HepatitisC genetic [37,38] (◇)	105	3	0.0076	0.5292
Krackhardt high tech [39] (△)	21	3	0.3873	22.596
Padgett-Florentine families [40] (<)	16	2	0.1458	19.957
Vickers-Chan 7th graders [41] (>)	29	3	0.4252	32.707
Lazega law firm [42] (▽)	71	3	0.2231	92.037

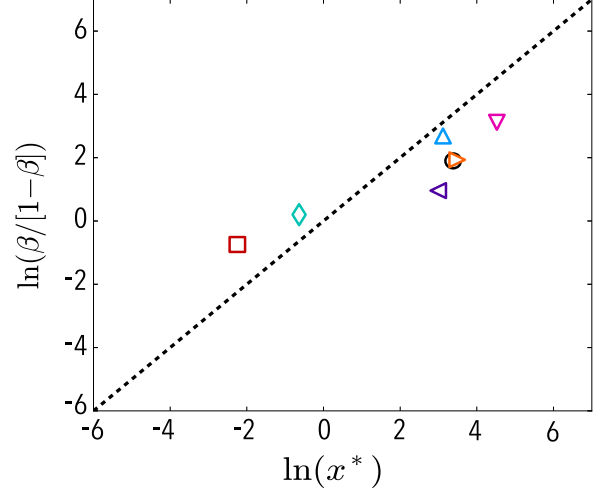


FIG. 8. $\ln[\beta/(1-\beta)]$ as a function of $\ln(x^*)$ for several real-world multiplex networks (see symbol code in Table I). Dashed line is Eq. (7).

We proceed as follows. First, since these networks are highly nonhomogeneous, we compute an *average sparsity* $\bar{\alpha}$. Then, with Eq. (8) we obtain the corresponding $x^* = x^*(N, M, \bar{\alpha})$ (see Appendix for details of the calculation of γ and δ). Therefore, we can already use Eq. (9) to predict the eigenfunction localization length of these networks that we will compare to the values of β computed directly from them. In Fig. 8 we report all data we obtained. Remarkably, although these real networks are binary multiplexed (basically different to the weighted multilayer networks used to derive the scaling of β) and highly nonhomogeneous, we observe a reasonably good general correspondence between the actual values of β (symbols) and the corresponding prediction (dashed line).

VI. CONCLUSIONS

Summarizing, in this study we have demonstrated that the normalized localization length β of the eigenfunctions of multilayer random networks scales as $x^*/(1+x^*)$. Here, $x^* = \gamma(b_{\text{eff}}^2/L)^\delta$; where b_{eff} is the effective bandwidth of the network's adjacency matrix, L is the adjacency matrix size, and $\delta \sim 1$. We showed that such scaling law is robust covering weighted multilayer and both weighted and unweighted node-aligned multiplex networks. Moreover, the scaling law was validated on real-world networks. Our results might shed additional light on the critical properties and structural organization of multilayer systems. Interestingly enough, our findings might be used to either predict or design (e.g, tune), by means of Eq. (9), the localization properties of the eigenfunctions of multilayer random networks. For instance, we anticipate the following cases: (i) Due to the banded nature of the adjacency matrices of the network models considered here, $b_{\text{eff}} < L$, it is unlikely to observe fully delocalized eigenfunctions unless the value of x^* is driven to large values, for example, by increasing the size of the subnetworks N and/or their sparsity α for a fixed value of M . (ii) For a fixed subnetwork size N and sparsity α , the eigenfunctions of the multilayer network become more localized when increasing the number of subnetworks M . We

hope our results motivate further numerical and theoretical studies.

ACKNOWLEDGMENTS

This work was partially supported by VIEP-BUAP (Grant No. MEBJ-EXC17-I), Fondo Institucional PIFCA (Grant No. BUAP-CA-169), and CONACyT (Grants No. I0010-2014/246246 and No. CB-2013/220624). F.A.R. acknowledges CNPq (Grant No. 305940/2010-4), FAPESP (Grants No. 2011/50761-2 and No. 2013/26416-9), and NAP eScience-PRP-USP for financial support. G.F.A. would like to acknowledge FAPESP (Grants No. 2012/25219-2 and No. 2015/07463-1) for the scholarship provided. Y.M. acknowledges support from the Government of Aragón, Spain through a grant to the group FENOL, by MINECO and FEDER funds (Grant No. FIS2014-55867-P) and by the European Commission FET-Proactive Project Multiplex (Grant No. 317532).

APPENDIX: SOME DETAILS ABOUT THE REAL-WORLD NETWORKS OF SEC. V

The methodology was applied to seven real networks, where two are biological networks and five from the social domain. The biological ones are constructed using the (BioGRID, thebiogrid.org) Biological General Repository for Interaction Datasets [37,38] and consider different types of interactions: (i) direct interaction, (ii) association, and (iii) physical association. On the other hand, regarding the social networks, each layer represents a different type of interaction: (i) on Pedgett-Florentine families [40], they are marriage alliances and business relationships; (ii) on Vickers-Chan 7th graders [41], they are based on the answer of three questions: “Who do you get on with in the class?” “Who are your best friends in the class?” “Who would you prefer to work with?”; (iii) on Lazega law firm [42], they are co-work, friendship, and advice; (iv) on Krackhardt high tech [39] they are advice, friendship and “reports to” and (v) on Kapferer tailor shop [36], they are “instrumental” (work and assistance related) and “societal” (friendships), recorded at two different times. For more information, please see their individual references on Table I.

In the main text, we tested the scaling law for β on the above real-world multiplex networks (see Fig. 8). Here, we give details regarding the calculation of γ and δ used to compute $x^* = x^*(N, M, \bar{\alpha})$. First note that since the real networks we are analyzing are binary multiplex, we use the unweighted multiplex model of Sec. IV B as the reference model. Also, recall that we have already obtained γ and δ for several values of α , indeed we used those values of γ and δ to produce the scaled curves of Fig. 7. However, in order to provide γ and δ corresponding to the specific values of

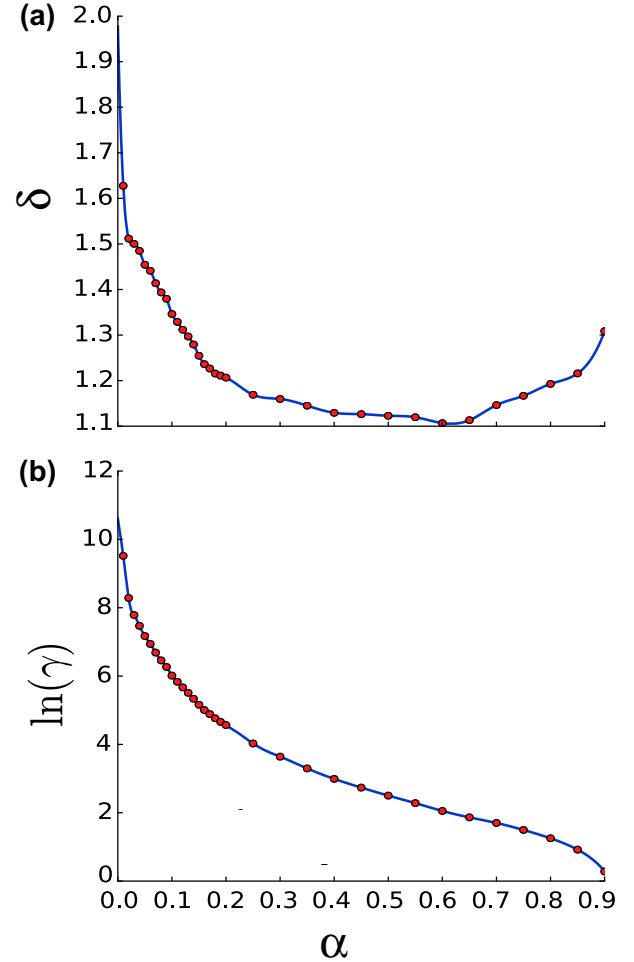


FIG. 9. (a) δ and (b) γ as a function of α for ensembles of unweighted multiplex networks (symbols). Continuous lines are cubic spline interpolations of the data.

$\bar{\alpha}$ of the real-world networks (see Table I), we proceed as follows. First, we consider the region of $\alpha < 0.2$, not explored in Sec. IV B. Again, we extract γ and δ from the fittings of the curves $\ln[\beta/(1-\beta)]$ versus $\ln(x)$ with Eq. (6). But, in contrast to the region $\alpha \geq 0.2$, where we performed the fittings in the fixed interval $\ln[\beta/(1-\beta)] = [0, 3.75]$, now we have to adjust the fitting interval because the linear behavior of the curves $\ln[\beta/(1-\beta)]$ versus $\ln(x)$ diminishes by decreasing α . Thus, in Fig. 9 we report the values of γ and δ obtained for $\alpha < 0.2$ (in steps of 0.01) and for $\alpha \geq 0.2$ (in steps of 0.05). Then, we perform a cubic spline interpolation (see continuous lines in Fig. 9); so, given a specific value of $\bar{\alpha}$ we retrieve interpolated values of γ and δ that we use to compute $x^* = x^*(N, M, \bar{\alpha})$ with Eq. (8).

- [1] M. Kivelä, A. Arenas, M. Barthelemy, J. P. Gleeson, Y. Moreno, and M. A. Porter, *J. Complex Netw.* **2**, 203 (2014).
 [2] E. Cozzo, G. F. Arruda, F. A. Rodrigues, and Y. Moreno, in *Multilayer Networks: Metrics and Spectral Properties* (Springer, Berlin, 2016), pp. 17–35.

- [3] *The Oxford Handbook of Random Matrix Theory*, edited by G. Akemann, J. Baik, and P. Di Francesco (Oxford University Press, New York, 2011).
 [4] For instance, the nearest-neighbor spacing distribution of the eigenvalues of the adjacency matrices of various model networks

- follow Gaussian Orthogonal Ensemble statistics [5]. In addition, the analysis of Erdős-Rényi networks shows that the level spacing distribution and the entropic eigenfunction localization length of the adjacency matrices are universal for fixed average degrees [6].
- [5] J. N. Bandyopadhyay and S. Jalan, *Phys. Rev. E* **76**, 026109 (2007).
- [6] J. A. Mendez-Bermudez, A. Alcazar-Lopez, A. J. Martinez-Mendoza, F. A. Rodrigues, and T. K. DM. Peron, *Phys. Rev. E* **91**, 032122 (2015).
- [7] R. J. Sánchez-García, E. Cozzo, and Y. Moreno, *Phys. Rev. E* **89**, 052815 (2014).
- [8] E. Cozzo and Y. Moreno, *Phys. Rev. E* **94**, 052318 (2016).
- [9] G. F. deArruda, E. Cozzo, T. P. Peixoto, F. A. Rodrigues, and Y. Moreno, *Phys. Rev. X* **7**, 011014 (2017).
- [10] A. V. Goltsev, S. N. Dorogovtsev, J. G. Oliveira, and J. F. F. Mendes, *Phys. Rev. Lett.* **109**, 128702 (2012).
- [11] S. Gómez, A. Díaz-Guilera, J. Gómez-Gardeñes, C. J. Pérez-Vicente, Y. Moreno, and A. Arenas, *Phys. Rev. Lett.* **110**, 028701 (2013).
- [12] M. L. Mehta, *Random Matrices* (Elsevier, Amsterdam, 2004).
- [13] G. Casati, L. Molinari, and F. M. Izrailev, *Phys. Rev. Lett.* **64**, 1851 (1990).
- [14] S. N. Evangelou and E. N. Economou, *Phys. Lett. A* **151**, 345 (1990).
- [15] Y. V. Fyodorov and A. D. Mirlin, *Phys. Rev. Lett.* **67**, 2405 (1991).
- [16] Y. V. Fyodorov and A. D. Mirlin, *Phys. Rev. Lett.* **69**, 1093 (1992).
- [17] A. D. Mirlin and Y. F. Fyodorov, *J. Phys. A: Math. Gen.* **26**, L551 (1993).
- [18] Y. V. Fyodorov and A. D. Mirlin, *Phys. Rev. Lett.* **71**, 412 (1993).
- [19] Y. F. Fyodorov and A. D. Mirlin, *Int. J. Mod. Phys. B* **8**, 3795 (1994).
- [20] F. M. Izrailev, *Chaos Solitons Fractals* **5**, 1219 (1995).
- [21] G. Casati, F. M. Izrailev, and L. Molinari, *J. Phys. A: Math. Gen.* **24**, 4755 (1991).
- [22] T. Kottos, A. Politi, F. M. Izrailev, and S. Ruffo, *Phys. Rev. E* **53**, R5553(R) (1996).
- [23] G. Casati, I. Guarneri, and G. Maspero, *J. Phys. I (France)* **7**, 729 (1997).
- [24] P. G. Silvestrov, *Phys. Rev. E* **55**, 6419 (1997).
- [25] T. Kottos, A. Politi, and F. M. Izrailev, *J. Phys.: Condens. Matter* **10**, 5965 (1998).
- [26] T. Kottos, F. M. Izrailev, and A. Politi, *Phys. D (Amsterdam)* **131**, 155 (1999).
- [27] W. Wang, *Phys. Rev. E* **65**, 066207 (2002).
- [28] G. Zhu, H. Yang, C. Yin, and B. Li, *Phys. Rev. E* **77**, 066113 (2008).
- [29] L. Gong and P. Tong, *Phys. Rev. E* **74**, 056103 (2006).
- [30] S. Jalan, N. Solymosi, G. Vattay, and B. Li, *Phys. Rev. E* **81**, 046118 (2010).
- [31] F. Passerini and S. Severini, in *Developments in Intelligent Agent Technologies and Multi-Agent Systems: Concepts and Applications*, edited by G. Trajkovski (IGI Global, Hershey, PA, 2011), Chap. 5, pp. 66–76.
- [32] G. Menichetti, D. Remondini, P. Panzarasa, R. J. Mondragon, and G. Bianconi, *PLoS ONE* **9**, e97857 (2014).
- [33] F. M. Izrailev, *Phys. Rep.* **196**, 299 (1990).
- [34] In the case of the multilayer network with layers on a line, when $\alpha = 0$ (i.e., when all vertices in the network are isolated), since the eigenfunctions of the adjacency matrices of Eq. (1) have only one nonvanishing component with magnitude equal to one, $\langle S \rangle = 0$ and $\beta \approx 2.07/L$. On the other hand, when all nodes in this multilayer network are fully connected we recover the GOE and $\langle S \rangle = S_{\text{GOE}}$. Thus, the *fully chaotic* eigenfunctions extend over the L available vertices in the network and $\beta = 1$.
- [35] To this end, we use exact numerical diagonalization to obtain eigenfunctions Ψ^l ($l = 1 \dots L$) of the adjacency matrices of large ensembles of multilayer random networks characterized by M , N , and α . We perform the average $\langle S \rangle$ taking half of the eigenfunctions, around the band center, of each adjacency matrix.
- [36] B. Kapferer, *Strategy and Transaction in an African Factory* (Manchester University Press, Manchester, 1972).
- [37] C. Stark, B.-J. Breitzkreutz, T. Reguly, L. Boucher, A. Breitzkreutz, and M. Tyers, *Nuc. Acids Res.* **34**, D535 (2006).
- [38] M. De Domenico, M. A. Porter, and A. Arenas, *J. Complex Netw.* **3**, 159 (2015).
- [39] D. Krackhardt, *Soc. Netw.* **9**, 109 (1987).
- [40] J. F. Padgett and C. K. Ansell, *Am. J. Sociol.* **98**, 1259 (1993).
- [41] M. Vickers and S. Chan, *Representing Classroom Social Structure* (Victoria Institute of Secondary Education, Melbourne, 1981).
- [42] E. Lazega, *The Collegial Phenomenon: The Social Mechanisms of Cooperation Among Peers in a Corporate Law Partnership* (Oxford University Press, Oxford, 2001).